Macromolecules

pubs.acs.org/Macromolecules Article

Structure and Organization of Amphiphilic Mikto-Grafted Molecular Brushes at Liquid/Liquid Planar Interfaces

Carlos A. Salinas-Soto, Carlos Padilla-Gutierrez, Margarita Herrera-Alonso, Esteban E. Ureña-Benavides, and Abelardo Ramírez-Hernández*

Cite This: *Macromolecules* 2024, 57, 2773−2785 Read Online

ACCESS | Metrics & More | Article Recommendations | Supporting Information

ABSTRACT: Amphiphilic molecular bottlebrushes provide a rich platform to develop emulsifiers for highly responsive emulsions. An understanding of the effect of the different molecular parameters on the structure, organization, and interfacial properties of bottlebrushes at oil/water interfaces is an important step toward the molecular engineering of advanced bottlebrush surfactants. In this work, extensive numerical simulations were performed to investigate the role of side chain and backbone lengths, as well as polymer surface concentration, on polymer structure, interfacial tension, and the organization of amphiphilic mikto-grafted molecular brushes at planar oil/water interfaces. Simulation results show that the side chain length is an important molecular parameter: long side chains favor extended conformations at low surface concentrations and higher local orientational order at high surface concentrations. In addition, regarding thermodynamic interfacial properties, simulation results predict that bottlebrushes with long side chains and short backbones are better at reducing interfacial tension compared to polymers with long backbones and short side chains, in agreement with previous experimental observations. Several structural descriptors were computed to provide a molecular view of the morphological changes occurring as the polymer surface concentration and molecular parameters were varied. The results reported here provide structure-interfacial property relations that will be useful to have a deeper understanding of how the molecular parameters of amphiphilic mikto-grafted molecular brushes will affect their behavior at oil−water interfaces to create advanced responsive emulsions.

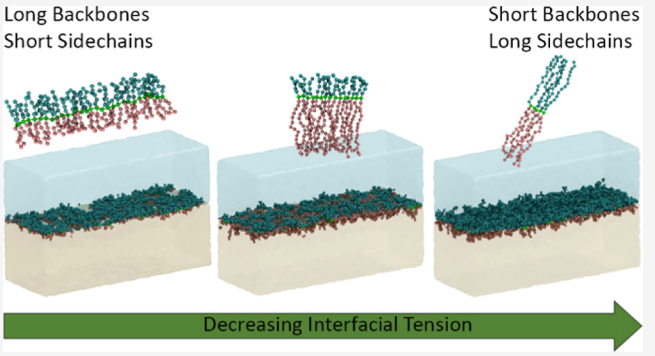

INTRODUCTION

Amphiphilic polymers provide a powerful and versatile platform for designing nanostructures suitable for a wide variety of applications, such as drug delivery,[1−4] photonic crystals,[5,6] and stabilization of emulsions for food,[7,8] cosmetic[9,10] and oil recovery applications.[11−13] Linear block copolymers have been widely studied as polymeric surfactants and emulsifiers due to their simple structure.[14−16] However, it has been found that polymers with complex architectures, such as star and bottlebrush polymers, have interesting and enhanced interfacial properties.[17−25] By using polyethylene oxide (PEO) star polymers, Li et al.[19] and Huang et al.[26] have shown that stable emulsions could be generated; they measured an interfacial tension reduction and an increased dilatational modulus induced by the presence of star polymers at the fluid interfaces. In a more recent work, Olszewski et al.[27] studied PEO stars with poly(divinylbenzene) cores at air/water and oil/water interfaces and found that the interface was viscoelastic at high polymer concentration, and it became elastic as the concentration was reduced; these star polymers were also effective emulsion stabilizers. On the other hand, Xie et al.[21] synthesized a series of heterografted bottlebrushes with hydrophobic poly(*n*-butyl acrylate) (PBA) and hydrophilic PEO side chains; polymer molecular parameters were varied to evaluate the bottlebrush performance as emulsion stabilizer. Xie et al. found that both the length of PEO side chains and their number fraction are important parameters; large values of these quantities produced stable xylene/water and cyclohexane/water emulsions. Importantly, they found that stable emulsions were possible even at surfactant concentrations as low as 0.005 wt %, when a bottlebrush with 17 wt % PEO was used; in contrast, a 6 wt % PEO bottlebrush only stabilized emulsions at a higher concentration of 0.02 wt % and above. Xie et al.'s experimental results also highlighted the importance of solvent-side chain interactions: by replacing xylene, a good solvent for PEO, by cyclohexane, which is a poor PEO solvent, the emulsifying efficiency of the bottlebrush was improved. The effect of the

Received: November 7, 2023
Revised: February 9, 2024
Accepted: February 27, 2024
Published: March 12, 2024

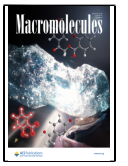

https://doi.org/10.1021/acs.macromol.3c02278
Macromolecules 2024, 57, 2773−2785

architecture was addressed by synthesizing a diblock copolymer and a star polymer with similar PEO content as that of the 17 wt % PEO bottlebrush; it was found that bottlebrush and star polymers formed stable emulsions at low concentrations (0.005%), whereas the diblock copolymer did not fully stabilize the emulsion at those concentrations.[21] All synthesized polymers were able to reduce interfacial tension; however, no correlation between emulsification efficiency and interfacial tension was found.

In a follow-up work, Hsieh et al.[28] performed interfacial rheology measurements with the goal of correlating emulsifying efficiency with molecular parameters associated with PBA−PEO bottlebrushes and the dilatational modulus. Pendant drop tensiometry was used to probe the dilatational rheology of a xylene/water interface with adsorbed PBA−PEO bottlebrushes. Six different bottlebrushes with varying PEO content and backbone length were synthesized: four polymers had high PEO content and similar PEO side chain length but different backbone lengths, the fifth polymer had similar PEO side chain lengths but a low PEO content, and finally, the last polymer had a low PEO content and a short side chain length. Two different polymer concentrations (0.005 and 0.1 wt %) were studied. It was found that the PEO content and backbone length have a strong effect on the reduction of the interfacial stress: polymers with high PEO content and short to intermediate backbone lengths greatly reduce interfacial tension when compared to polymers with long backbones and low PEO content. The interfacial rheology results seem to suggest that the most efficient bottlebrush emulsifiers are those that produce interfacial stiffening (high compressional modulus).[28]

More recently Seong et al.[29] synthesized bottlebrush random copolymers composed of PEO and poly(dimethylsiloxane) (PDMS) as side chains and studied the self-assembly and adsorption kinetics of these polymers at toluene/water interfaces. These authors also investigated the role of the backbone degree of polymerization, N_{bb}, and grafting density, σ, on the interfacial tension. They found that for fully grafted polymers with symmetric composition ($f_{POE} = 0.5$), the larger N_{bb} is, the less reduction of interfacial tension is achieved. However, the interfacial tension vs time plots displayed in ref 29 seem to indicate that a steady state was not reached within the experimental time window; thus, a possible explanation of the observed behavior could be related to the slow diffusion of polymers with large N_{bb}; thus, the effect of N_{bb} on the interfacial tension is still an open question. It was also reported that, at very low grafting densities, bottlebrush polymers lost interfacial activity.[29]

Given the complexity of bottlebrush polymers and all different molecular parameters associated with them, as well as those of liquid/liquid interfaces, it becomes a challenge to explore all possible parameters from an experimental perspective. Computational modeling could provide physical insights about the relevant molecular parameters involved in the self-assembly and thermodynamics of bottlebrush polymers at liquid/liquid interfaces. Simulation work on linear and ring polymers,[30] as well as polymer-grafted particles[31] at liquid/liquid interfaces has been reported extensively; however, to the best of the authors' knowledge, there are very few works on bottlebrush polymers at liquid/liquid interfaces. Bugaeva et al.[32] studied the adsorption kinetics of bottlebrushes at a liquid/liquid interface using Dissipative Particle Dynamics. They simulated amphiphilic bottlebrushes with alternating hydrophilic and hydrophobic side chains and varied the backbone length and hydrophobic/hydrophilic ratio in the bottlebrush polymer. They found that bottlebrushes at the water phase self-assembled into spherical micelles, which unfolded into a worm-like morphology as they adsorbed at the interface. They also observed that the rate of adsorption to the interface depends mostly on the length of the hydrophobic side chain and very little on the backbone length and the hydrophilic/hydrophobic ratio. Interestingly, Bugaeva et al. also found that when the interface is under compression, a spherical to cylindrical morphological transition takes place.

In an important simulation work reported by Moghimikheirabadi et al.,[33] the structure and surface rheology of two symmetric linear triblock copolymers at a water/vapor interface were investigated. Polymer concentration was varied, and two different polymer compositions were studied: one of the polymers had two long hydrophilic blocks at the chain ends and a short hydrophobic block in the middle; the other polymer had two short hydrophobic blocks at the ends and a long hydrophilic block in the middle. Both equilibrium and nonequilibrium molecular dynamics (NEMD) were performed; nonbonded interactions were represented by the Lennard-Jones potential, and bonded interactions were modeled by the FENE potential. Their simulations showed that the more hydrophilic triblock copolymer gave rise to a higher surface pressure to the interface at a fixed surface concentration and displayed a larger radius of gyration compared to the less hydrophilic triblock. Moghimikheirabadi et al. found that the interfacial tension reduces faster, as a function of surface concentration, for the polymer with long hydrophilic blocks than for short hydrophilic blocks. They also introduced a methodology to study surface dilatational rheology. They found that by increasing the surface concentration, both the dilatational storage and loss moduli increase.[33] These results helped to explain and rationalize previous experimental observations done by the same authors.[34] This previous simulation work highlights the importance of modeling approaches to understand the relationship between the structure and organization of polymers at the liquid/liquid interface and the associated thermodynamic and surface rheological properties.

As described above, the interfacial properties of bottlebrushes depend greatly on their architectural parameters. Thus, an understanding of the effect of these parameters on the effectiveness of stabilizing liquid/liquid interfaces is an important step toward the molecular engineering of advanced surfactants and emulsifiers. Numerical simulations are powerful as they can provide a prediction of the behavior before synthesis, saving time and reducing costs, as well as having advantages, such as the ease of tuning architectural and chemical parameters of the polymer. In this work, we used a coarse-grained model and performed extensive numerical simulations using dissipative particle dynamics (DPD) to investigate how architectural parameters of mikto-grafted bottlebrushes, such as side chain and backbone lengths, as well as surface concentration, affect conformations and organization of bottlebrushes at planar liquid/liquid interfaces; the dependence of thermodynamic properties such as interfacial tension and surface pressure on the architectural parameters was also investigated.

MODEL AND METHODS

A coarse-grained model was employed to represent mikto-grafted bottlebrushes since the time and length scales of interest are beyond the ones that could be explored by atomistic modeling. This model contains information on the molecular architecture of the bottlebrushes, and chemical details are encoded into soft generic intermolecular

https://doi.org/10.1021/acs.macromol.3c02278
Macromolecules 2024, 57, 2773−2785

interaction parameters.[35−37] Macromolecules are represented by a bead−spring model (Figure 1), and the DPD formalism was used to

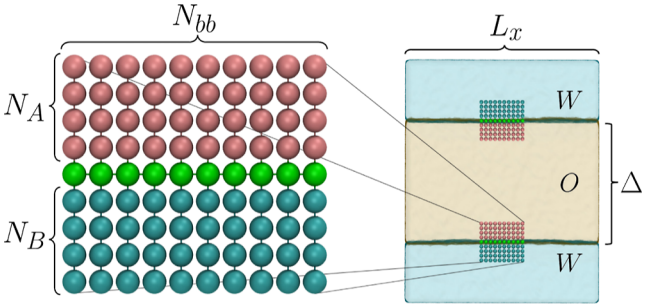

Figure 1. Left: schematic representation of the mikto-grafted bottlebrush architecture considered in this work, backbone beads (green) are connected to hydrophobic side chains (pink) and hydrophilic side chains (blue). Right: schematic of the simulation setup. The oil phase with thickness Δ is placed in the middle of the simulation box creating two O/W interfaces. Macromolecules are generated randomly at both interfaces with the same number of polymers per interface.

simulate bottlebrushes at oil−water (O/W) interfaces. DPD is a mesoscopic simulation technique introduced by Hoogerbrugge and Koelman[38] and modified by Español and Warren[39] and Groot and Warren.[40] Since it uses soft molecular interactions, larger time steps can be used, and the computational cost is lower than atomistic simulations; it is common to use this technique to investigate the properties of block copolymers in solution.[41−49]

As discussed by Xie et al.,[21] in the design of well-defined heterografted molecular brushes, several factors need to be considered: side chain lengths, composition, grafting density, and backbone length. In this work, three parameters were varied: (i) side chain length, (ii) backbone length, and (iii) polymer surface concentration, Γ. In a previous work, we investigated the solution self-assembly of amphiphilic mikto-grafted bottlebrushes in a selective solvent in the low concentration limit.[50,51] In this work, the same model is adopted; bottlebrushes are represented by a bead−spring model composed of identical macromonomers, as shown in Figure 1: each macromonomer is a linear triblock ACB, composed by N_A beads (hydrophobic side chain), N_B beads (hydrophilic side chain), and one backbone bead type C. This macromonomer is repeated, creating an amphiphilic bottlebrush polymer of length N_{bb} (see Figure 1). Oil and water phases have been included explicitly in simulations and are represented by beads type W (water) and type O (oil). DPD reduced units were used, where r_c is the unit length, describing the diameter of a single bead, and k_BT is the energy unit. The simulation box has the dimensions of $L_x = L_y = 80r_c$ and $L_z = 100r_c$. To create the two-phase system, molecules of the oil phase were initialized randomly within a layer of thickness Δ, placed in the middle of the simulation box, and water molecules were initialized randomly outside of the oil layer, thus creating two planar O/W interfaces (Figure 1). The thickness of the oil layer was chosen to be $\Delta = 50r_c$ to minimize the interface−interface interaction. Bottlebrushes were placed randomly at the interfaces, with the same number of polymers per interface. Surface concentration (adsorption), Γ, was defined as the number of macromonomers per unit area, with the interfacial area $A = L_x \cdot L_y$; thus, $\Gamma = N_{bb}N_c/A$, where N_c is the number of polymers per interface; Γ has units of r_c^{-2}.

Intramolecular interactions between two bonded beads are given by $u_{intra} = \frac{k_2}{2}(r_{ij} - l_0)^2$, where the bond coupling constant is denoted by k_2, the equilibrium bond length is l_0, and the distance between two particles is r_{ij}. Being consistent with our previous work,[50,51] the following values were selected: $l_0 = 0.75r_c$ and $k_2 = 128k_BT/r_c^2$, k_B is the Boltzmann constant, and T is the temperature. Side chains and backbone are modeled as fully flexible chains; therefore, no bending potential interaction was used. Nonbonded interactions are governed by soft potentials. The effective intermolecular force that bead i feels due to the interaction with bead j is given by $\mathbf{F}_{ij} = \mathbf{F}_{ij}^C + \mathbf{F}_{ij}^D + \mathbf{F}_{ij}^R$, which contains three different contributions: the conservative force, $\mathbf{F}_{ij}^C = a_{ij}(1 - r_{ij}/r_c)\hat{\mathbf{r}}_{ij}$, the dissipative force, $\mathbf{F}_{ij}^D = -\xi(1 - r_{ij}/r_c)^2(\mathbf{v}_{ij}\cdot\hat{\mathbf{r}}_{ij})\hat{\mathbf{r}}_{ij}$, and a stochastic force, $\mathbf{F}_{ij}^R = \varphi(1 - r_{ij}/r_c)\theta_{ij}\frac{1}{\sqrt{\Delta t}}\hat{\mathbf{r}}_{ij}$, all of them vanish for $r_{ij} > r_c$. In the previous equations, $\hat{\mathbf{r}}_{ij}$ is the unit vector between particles i and j, $\mathbf{v}_{ij} = \mathbf{v}_i - \mathbf{v}_j$ is the relative velocity of the two interacting particles, and ξ and φ represent the strength of dissipation and fluctuation, respectively.[40] In order for the local momentum to be conserved, the random force has a symmetry property, $\theta_{ij} = \theta_{ji}$, and ξ and φ are related by the fluctuation−dissipation theorem:[39] $\varphi^2 = 2\xi k_BT$. In this work, the standard values of $\xi = 4.5$ and $\varphi = 3$ were used. Interaction parameters a_{ij} are used to quantify the strength of the repulsion between the beads. These parameters are related to the Flory−Huggins parameter,[40] χ_{ij} by $a_{ij} = a_{ii} + 3.497\chi_{ij}$, where a_{ii} is the self-interaction parameter, selected as $a_{ii} = 25$ for a reduced density $\rho = 3$.[40] The χ_{ij} parameters can be acquired from experimental measurements, estimated using solubility parameters, or through MD simulations.[52] The interaction parameters in this work represent amphiphilic bottlebrush polymers at the interface between two highly incompatible liquids; the intermolecular interactions among every pair of chemical species, a_{ij}, are given by

	A	B	C	W	O
A	25				
B	35	25			
C	25	35	25		
W	50	25	50	25	
O	25	50	25	100	25

All simulations were performed using HOOMD-Blue.[53,54] The time step used to integrate the equations of motion was set at $\delta t = 0.01\tau$, where $\tau = \sqrt{r_c m/k_BT}$ and $m = 1$ is the mass of a DPD bead. VMD[55] was used to visualize the dynamic evolution of the bottlebrushes at the interface. Simulations were performed on a box of volume $L_x \times L_y \times L_z$, as described in Figure 1, and periodic boundary conditions were imposed in all directions. In this work, we are interested in the behavior of amphiphilic bottlebrushes at oil/water interfaces and the effects of the architectural parameters (N_{bb}, N_A, and N_B) on the morphological properties of the polymer and the thermodynamics of the interface. Thus, we studied three backbone lengths, $N_{bb} = 5$, 15, 30, and explored two cases regarding side chain lengths: symmetric side chains ($N_A = N_B = 5$, 15) and asymmetric side chains ($N_A = 15$, $N_B = 5$). All systems were initially relaxed for 10^4 timesteps with $a_{ij} = 25$ for all pairs, except for $a_{OW} = 100$, where the highly repulsive interaction between oil and water is to avoid mixing. After this step, all values of a_{ij} were set as in the matrix above, and simulations were run for 10^7 timesteps.

Postprocessing analysis of trajectories was performed using MDAnalysis[56,57] to calculate the gyration tensor associated with each polymer, given by[58]

$$G_{\alpha\beta} = \frac{1}{M}\sum_k (r_k^\alpha - R_{com}^\alpha)(r_k^\beta - R_{com}^\beta) \quad (1)$$

where r_k^α is the spatial coordinate of the k-th bead, and R_{com}^α is the associated coordinate of the center of mass of the molecular brush; the sum goes over all polymer beads in the molecular brush. Morphological properties, such as the radius of gyration, R_g, and the shape anisotropy parameter, A_3, were computed. The radius of gyration characterizes the size of the polymer as a whole, and the shape anisotropy parameter is a quantification of the shape of the polymer, taking values between zero and one, where values close to zero represent spherical shapes while values close to one represent rods.[59] These morphological properties were obtained from the eigenvalues of the gyration tensor,[60] with the radius of gyration defined as $R_g^2 \equiv \lambda_1 + \lambda_2 + \lambda_3$, where λ_i are the eigenvalues of $G_{\alpha\beta}$, and the shape anisotropy parameter is defined as $A_3 = 1 - 3\frac{\lambda_1\lambda_2 + \lambda_2\lambda_3 + \lambda_1\lambda_3}{(\lambda_1 + \lambda_2 + \lambda_3)^2}$. The end-to-end distance of the backbone was obtained by calculating the length of the vector that goes from one

https://doi.org/10.1021/acs.macromol.3c02278
Macromolecules 2024, 57, 2773−2785

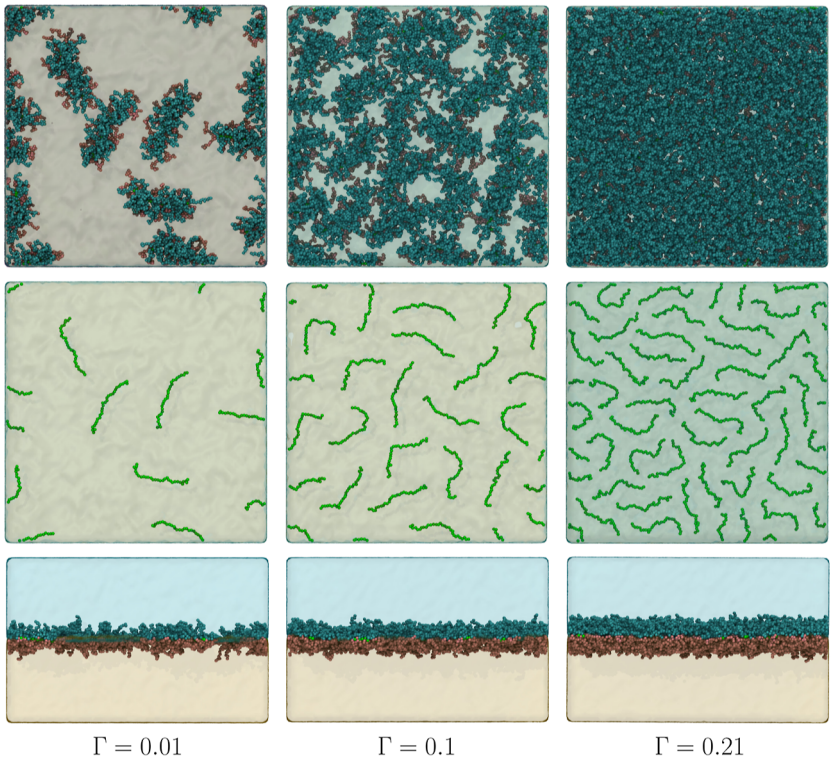

Figure 2. Bottlebrush polymers at a liquid−liquid interface for three different values of surface concentration, Γ, for N_{bb} = 30 with $N_A = N_B$ = 15. Upper row: top-view displaying backbone and side chains beads. Central row: top-view with only backbone beads. Bottom row: cross-section view of the interface. Oil and water beads are not displayed for clarity. As can be noticed, the interface saturates as the concentration increases, backbones adopt more elongated configurations at low concentration, and side-chains seem to orient perpendicular to the interface as surface concentration increases.

extreme of the backbone to the other. End-to-end distances of side chains were computed from the length of the vector from the bead that is attached to the backbone to the end bead of the side chain and decomposed into their component parallel to the interface, $R_{\parallel}$ (xy plane), and their component perpendicular to the interface, $R_{\perp}$ (z-axis). The interfacial tension of the O/W interface was computed through the pressure tensor, which is calculated by HOOMD-Blue[54] using

$$P_{\alpha\beta} = \left[\sum_{k=1}^{N} m_k v_k^{\alpha} v_k^{\beta} + \sum_{k=1}^{N} \sum_{l>k} \frac{1}{2} (r_{kl}^{\alpha} F_{kl}^{\beta} + r_{kl}^{\beta} F_{kl}^{\alpha}) \right] / V \tag{2}$$

where N is the total number of particles, V is the volume, m_k is the mass of the k-th particle, v_k^{α} is the α-component of the velocity vector, and the components of the Virial tensor are defined as $r_{kl}^{\alpha} F_{kl}^{\beta}$, where r_{kl}^{α} is the α-component of the vector separating particles k, l, and F_{kl}^{β} is the β-component of the pairwise force between particles k, l. At equilibrium, the interfacial tension can be defined through the diagonal elements of the pressure tensor[61]

$$\gamma_{int} = \frac{L_z}{2} \left\{ \langle P_{zz} \rangle - \frac{1}{2} [\langle P_{xx} \rangle + \langle P_{yy} \rangle] \right\} \tag{3}$$

where the brackets represent ensemble average; this expression is only valid for planar interfaces. We also aimed to quantify the organization of polymers at the interface, which was done by computing the orientational tensor Q, whose elements are given by[62]

$$Q_{\alpha\beta} = \frac{1}{2N_c} \sum_{i} (3u_i^{\alpha} u_i^{\beta} - \delta_{\alpha\beta}) \tag{4}$$

where N_c is the total number of polymers at a given interface, u_i^{α} is the α-component of the unit vector along the backbone of the polymer i, which in our work is defined as the backbone end-to-end vector divided by its magnitude, and δ_{ij} is the Kronecker's delta. The order parameter, S, is the largest positive eigenvalue of tensor Q. The corresponding eigenvector, $\hat{n}$, is the director and points in the average direction of the chains. Finally, we computed the molecular area $\hat{A}$ defined as $\hat{A} = 1/\Gamma$, as well as the interfacial pressure $\Pi = \gamma_0 - \gamma_{int}$, where γ_0 is the interfacial tension of the O/W interface with no adsorbed polymers.

As mentioned above, three different backbone lengths N_{bb} of 5, 15, and 30 were studied, and ten different values of Γ, ranging from 0 to 0.21, were simulated for each case. The numbers of polymers per interface used in simulations are listed in the Supporting Information. For each of these values of Γ, three cases were simulated: symmetric side chains with $N_A = N_B$ = 5 and 15 and asymmetric side chains N_A = 15 and N_B = 5; a total of 90 simulations, each containing 1.92 million particles, were performed. Polymer properties reported below, e.g., $\langle R_g \rangle$, are time average and average over-all polymers. Given that the systems were initialized with polymers placed at the interfaces already, and because of DPD's intrinsic soft potentials, the relaxation is quite fast (see Figure S14, Supporting Information, for a plot of the potential energy as a function of time): structural properties display well-defined average values, but the first two million steps were discarded from time-averaging. Thus, all time-average calculations were performed using system configurations, saved every 20,000 timesteps, in the last 8×10^6 steps.

RESULTS AND DISCUSSION

Visual Observations. The first task was to elucidate how architectural parameters (N_{bb}, N_A, and N_B) and surface concentration, Γ, influence polymer structure and organization at the liquid−liquid interface. Figure 2 displays representative instantaneous conformations of bottlebrushes at one interface for three different values of Γ. The upper row presents a top-view of the interface, displaying both side chains and backbones; the same top-view but only displaying backbone beads is shown in the central row; and a cross-section view displaying all beads is shown at the bottom row. These snapshots were taken from a polymer system with N_{bb} = 30 and $N_A = N_B$ = 15, for three values

https://doi.org/10.1021/acs.macromol.3c02278
Macromolecules 2024, 57, 2773−2785

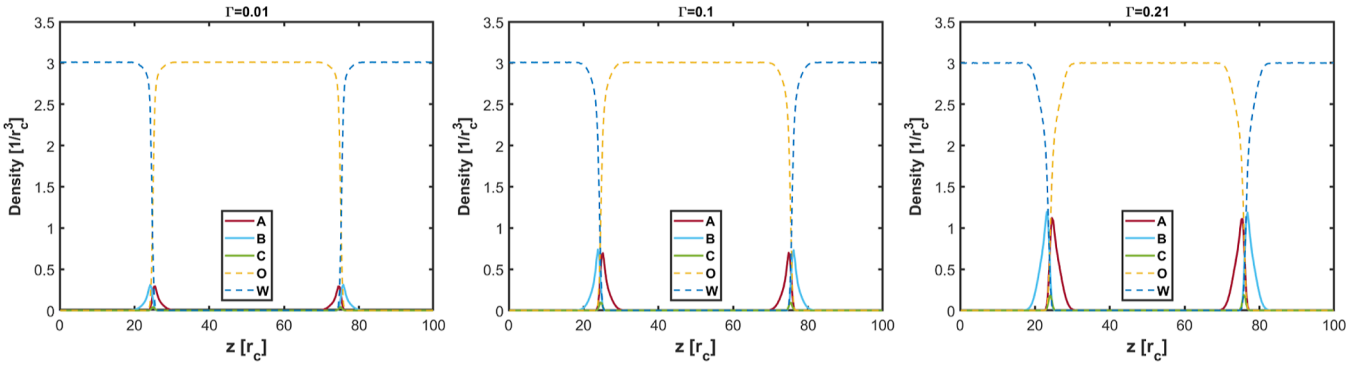

Figure 3. Density profiles, $\rho(z)$, along the direction perpendicular to the oil−water interfaces, for the different components, as described by the labels. Plots are for three different surface concentrations: (left) $\Gamma = 0.01$, (center) $\Gamma = 0.1$, and (right) $\Gamma = 0.21$. Note the increase of the distribution's width for the polymer components as Γ increases. $N_{bb} = 30$ with $N_A = N_B = 15$; expression between brackets are units of the respective quantity.

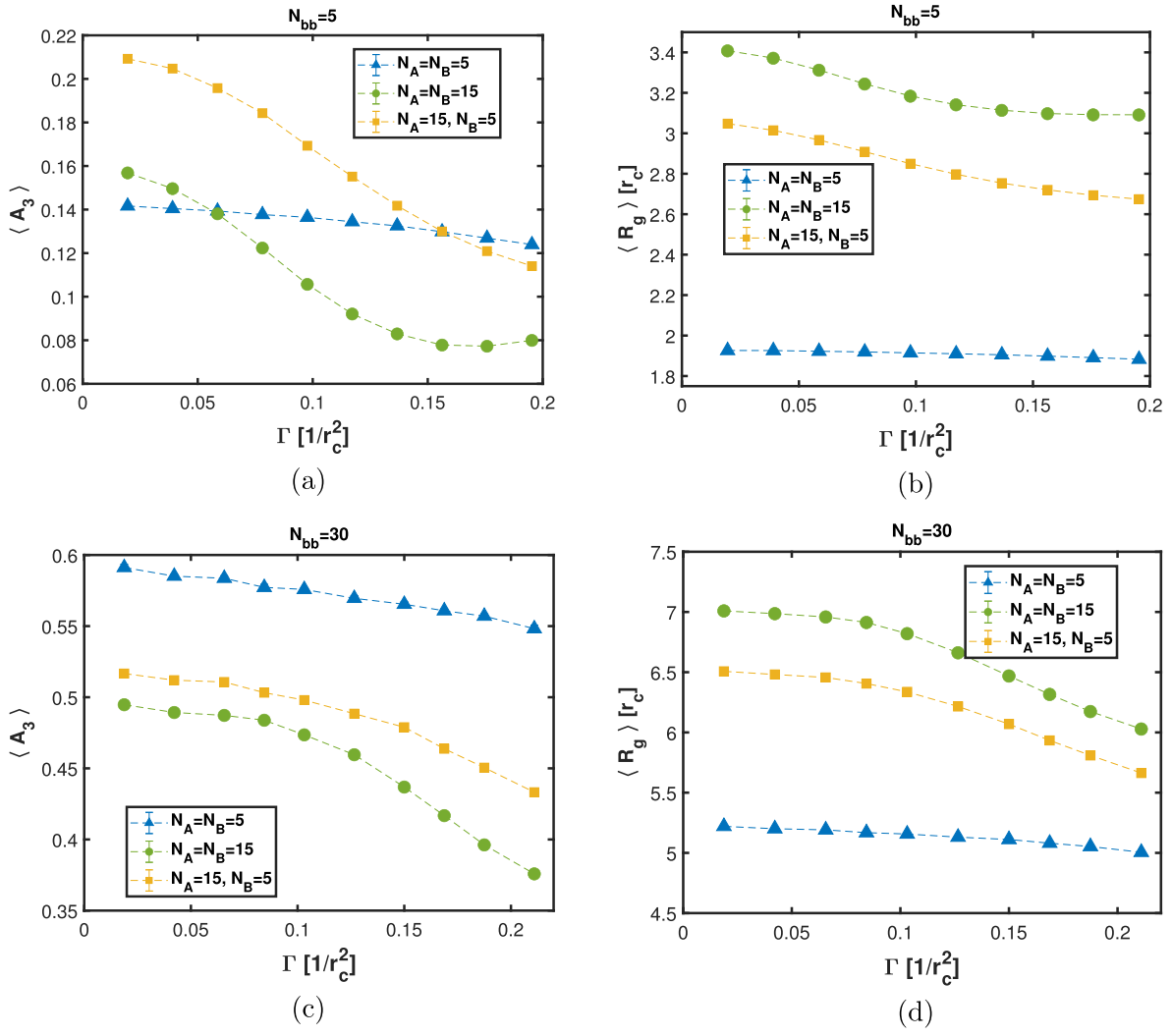

Figure 4. Evolution of the shape anisotropy $\langle A_3 \rangle$ and the radius of gyration $\langle R_g \rangle$ of bottlebrush polymers with increasing surface concentration, Γ, and different architectural parameters, as indicated by the labels. Top row: backbone molecular weight $N_{bb} = 5$. Bottom row: backbone molecular weight $N_{bb} = 30$. The error bars are smaller than the symbols. An increase in surface concentration reduces the value of both structural descriptors; however, for short symmetric side chains with $N_A = N_B = 5$, a weaker dependence on Γ is observed. Polymers with short backbones display ellipsoidal/spherical morphologies, $A_3 \leq 0.2$, whereas polymers with long backbones adopt cylindrical conformations, $0.3 \leq A_3 \leq 0.7$. The anisotropy parameter A_3 is unitless.

of surface concentration (total number of the backbone repeating units per interfacial area): $\Gamma = 0.01$, 0.1, and 0.21. Figures S1 and S2 in the Supporting Information show instantaneous conformations for symmetric side chains with length $N_A = N_B = 5$ and asymmetric side chains with $N_A = 15$, $N_B = 5$, for a backbone length of $N_{bb} = 30$.

https://doi.org/10.1021/acs.macromol.3c02278
Macromolecules 2024, 57, 2773−2785

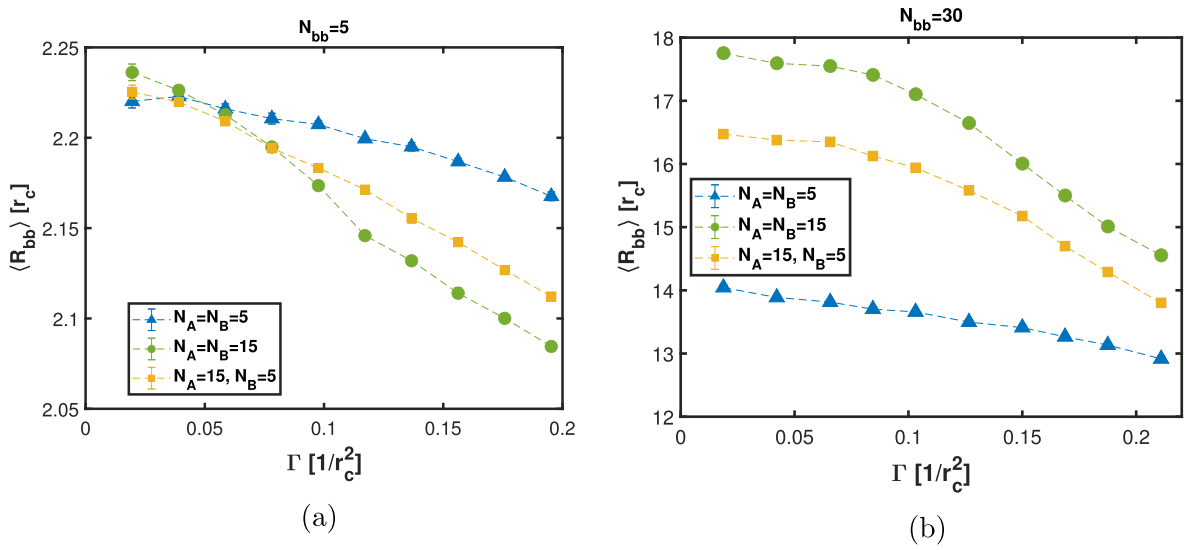

Figure 5. Evolution of end-to-end distances, $\langle R_{bb}\rangle$, of brush polymer backbones with increasing surface concentration, Γ, and different architectural parameters, as indicated by the labels, for two different backbone lengths (a) $N_{bb} = 5$ and (b) $N_{bb} = 30$. As can be noticed, $\langle R_{bb}\rangle$ decreases as Γ increases, and the reduction is larger for long backbones and long side chains.

A few observations can be made by looking at the snapshots: first, at low surface concentrations molecular brushes adopt elongated cylindrical morphologies; in this diluted limit, both A and B side chains interact with side chains within the same molecule and their respective good solvents. Under this condition, excluded volume interactions give rise to a large effective Kuhn length that is strongly dependent on the side chain molecular weight.[63−65] This effect is also enhanced because of the reduction of the exposed oil−water interfacial area if bottlebrushes adopt extended conformations with side chains lying mostly parallel to the interface, as observed in the snapshots. As the interface saturates, by increasing Γ, intermacromolecular interactions start to dominate and polymers display more compact morphologies, with backbones displaying both elongated and folded conformations (Figure 2, right). This can be understood by considering that, as the polymer surface concentration increases (transitioning from a semidilute to a concentrated regime), excluded volume interactions are screened and chains behave as if they were in a theta or melt condition,[66] with a reduced effective Kuhn length. This phenomenology is also observed for bottlebrushes with asymmetric side chains ($N_A = 15$, $N_B = 5$, Figure S1) and short symmetric side chains ($N_A = N_B = 5$, Figure S2). However, note that for short side chains, the effective Kuhn length is smaller in the low-concentration regime, as expected,[63] and more coiled conformations are observed. In addition, short side chains are not long enough to saturate the interface, and polymers remain in the semidilute regime. The asymmetric bottlebrushes possess hydrophobic side chain lengths of $N_A = 15$, long enough to reach concentrated conditions at large Γ. These effects were quantified by computing the morphological properties described below.

The bottom row of Figure 2 shows cross-sectional views of the top interface. As can be seen, as Γ increases and intermacromolecular interactions become dominant, side chains stretch away from the interface to avoid overlapping, an expected behavior for polymer brushes at high-coverage on an interface.[67] This is reflected in the behavior of the density profiles in Figure 3; there, it can be noticed that the densities' width for the polymer components increases as Γ increases. As expected, the longer the side chains are, the larger the thickness of the polymer layer is, as it is nicely illustrated by the density profiles in Figures S3 and S4 corresponding to symmetric side chains with length $N_A = N_B = 5$ and asymmetric side chains with $N_A = 15$, $N_B = 5$, respectively, for a backbone length of $N_{bb} = 30$. The qualitative description given so far will now change to a quantitative analysis of the structure and organization of the molecular brushes at the oil−water interface.

Morphology of Polymers at the Interface. Regarding polymer structure, several quantities were computed: radius of gyration, relative shape anisotropy, and end-to-end distances for both backbones and side chains. The evolution of the average shape anisotropy parameter, $\langle A_3\rangle$, with increasing surface concentration and different architectural parameters is shown in Figure 4a,c for molecular brushes with $N_{bb} = 5$ and 30, respectively. The plot of $\langle A_3\rangle$ vs Γ for $N_{bb} = 15$ is presented in Figure S6. The values of A_3 range between 0 and 1, with values close to zero indicating spherical morphologies, whereas values close to one describe elongated, rod-like structures.[59] As can be seen in Figure 4a, the average values of the shape anisotropy parameter, $\langle A_3\rangle$, are in the range [0.12, 0.14] for the symmetric molecular brush with the shorter side chain lengths $N_A = N_B = 5$; these values of the anisotropy parameter indicate that these polymers adopt spherical/ellipsoidal conformations (Figure S5 supports this). For this short side chain length, $\langle A_3\rangle$ displays little variation as surface concentration is increased. This weak dependence on Γ was present in all structural descriptors when both side chains were short. For example, for the largest backbone, $N_{bb} = 30$, when $N_A = N_B = 5$ and $\langle A_3\rangle \approx 0.59$ at the lowest surface concentration and slightly reduced to $\langle A_3\rangle \approx 0.55$ at the largest Γ value; these values of the shape anisotropy parameter indicate that these polymers adopt cylindrical conformations (as shown in Figure S2). The error bars displayed in all figures were obtained by using the block average method,[68] and they correspond to the quantity $\sigma_X/\sqrt{n-1}$, where n is the number of blocks $\sigma_X \equiv \sqrt{\langle X^2\rangle - \langle X\rangle^2}$, thus providing a measure of the statistical error in the quantity X. In the case of bottlebrushes with longer side chains, both symmetric and asymmetric, a stronger dependence on Γ is observed (see Figure

https://doi.org/10.1021/acs.macromol.3c02278
Macromolecules 2024, 57, 2773−2785

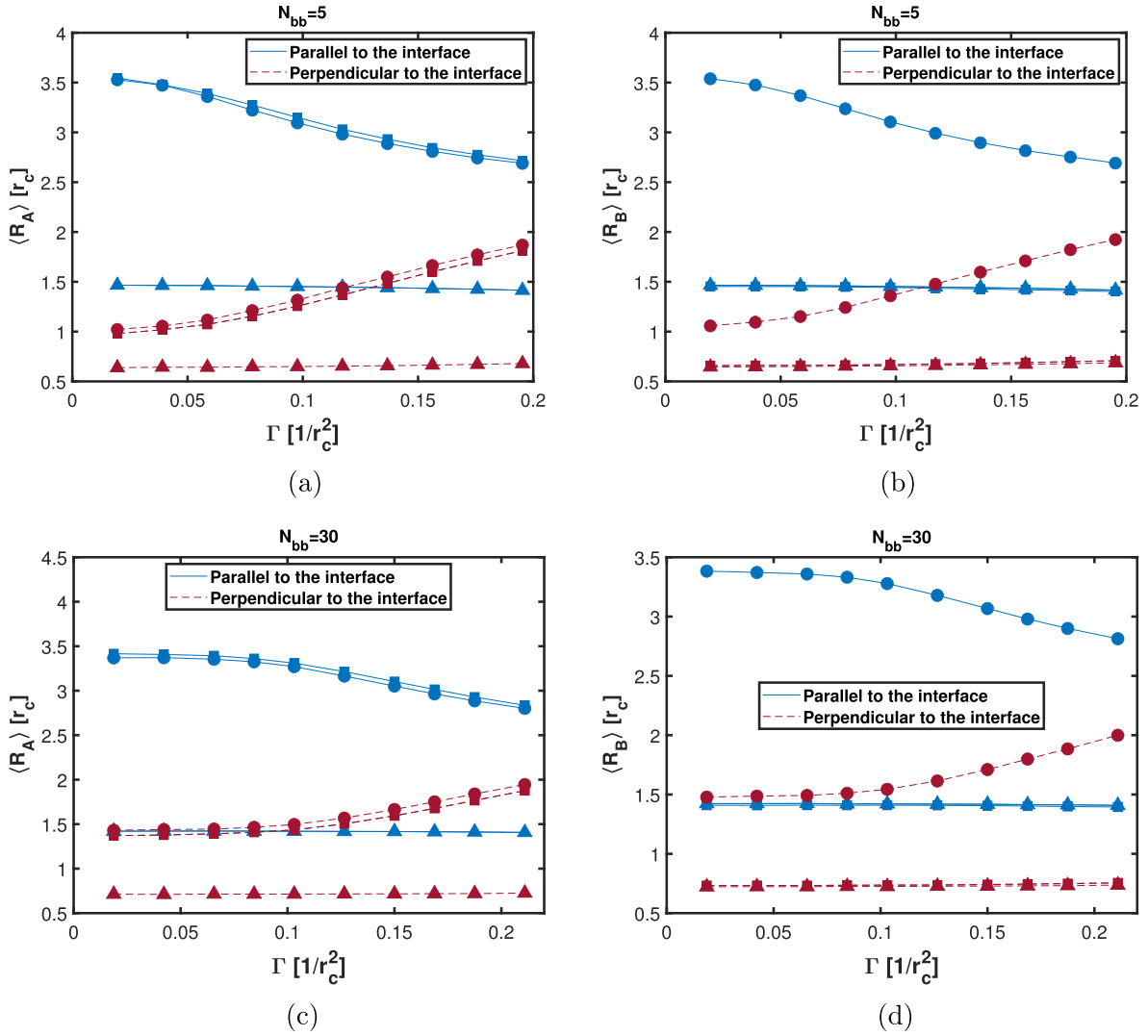

Figure 6. Parallel (red dashed) and perpendicular (blue continuous) components of side chain end-to-end vectors with increasing surface concentration. $N_A = N_B = 5$ (triangles), $N_A = N_B = 15$ (circles), and $N_A = 15$, $N_B = 5$ (squares). (a,c) correspond to side chains type *A*, for $N_{bb} = 5$ and $N_{bb} = 30$, respectively. (b,d) correspond to side chains type *B*, for $N_{bb} = 5$ and $N_{bb} = 30$, respectively. The error bars are smaller than the symbols.

4a,c). Notice that bottlebrushes with $N_{bb} = 5$ and $N_A = 15$, $N_B = 5$ or $N_A = N_B = 15$ can be seen as star-like polymers; for these two cases, $\langle A_3 \rangle$ decreases monotonically as Γ increases, but the symmetric bottlebrush adopts morphologies that are more spherical, due to its symmetric nature, compared to the asymmetric polymer (Figure 4a). The same stronger dependence on Γ can be observed for longer backbones, as can be seen in Figure 4c for brush polymers with $N_{bb} = 30$: as the interface saturates, brush polymers transit from configurations with extended backbones to configurations where the backbone adopts folded configurations. This qualitative change in conformations is reflected by a reduction of $\langle A_3 \rangle$ as the surface concentration increases. The radius of gyration (right column in Figure 4) also displays a monotonic decrease as the interface is populated with brush polymers. The stronger reduction occurs for bottlebrushes with longer backbones and longer side chains (Figure 4d), whereas symmetric polymers with short side chains display little variation with surface concentration. Note that, as expected, the longer the side chains are, the greater $\langle R_g \rangle$ is. The reduction of $\langle R_g \rangle$ as Γ increases is a reflection of the more compact morphologies adopted by polymer brushes as they interact with one another.

End-to-end distances associated with the backbone of each bottlebrush, R_{bb}, were also calculated. In the star-like limit, $N_{bb} = 5$, the backbone average end-to-end distance $\langle R_{bb} \rangle$ displays little variation as a function of Γ, as seen by the length scale of Figure 5a as it goes from $R_g \approx 2.25$ to $R_g \approx 2.1$. There is a clear tendency to lower $\langle R_{bb} \rangle$ values as surface concentration increases, which becomes more pronounced for bottlebrush polymers with long side chains; however, the variation is not significant. On the contrary, brush polymers with large backbones, $N_{bb} = 30$, display a more appreciable change (Figure 5b). As mentioned previously, in the low concentration limit, excluding volume interactions between side chains gives place to an effective backbone Kuhn length that increases with side chain degree of polymerization, therefore giving place to more extended backbones (larger $\langle R_{bb} \rangle$ values) for symmetric bottlebrushes with $N_A = N_B = 15$. Symmetric bottlebrushes with short side chains have a smaller effective Kuhn length, and the backbone extends less. The $\langle R_{bb} \rangle$ values for the asymmetric polymers are located between these two limits.

As the concentration increases and polymers begin to interact with each other, excluded volume interactions are screened, and the effective Kuhn length reduces, giving place to more flexible

https://doi.org/10.1021/acs.macromol.3c02278
Macromolecules 2024, 57, 2773−2785

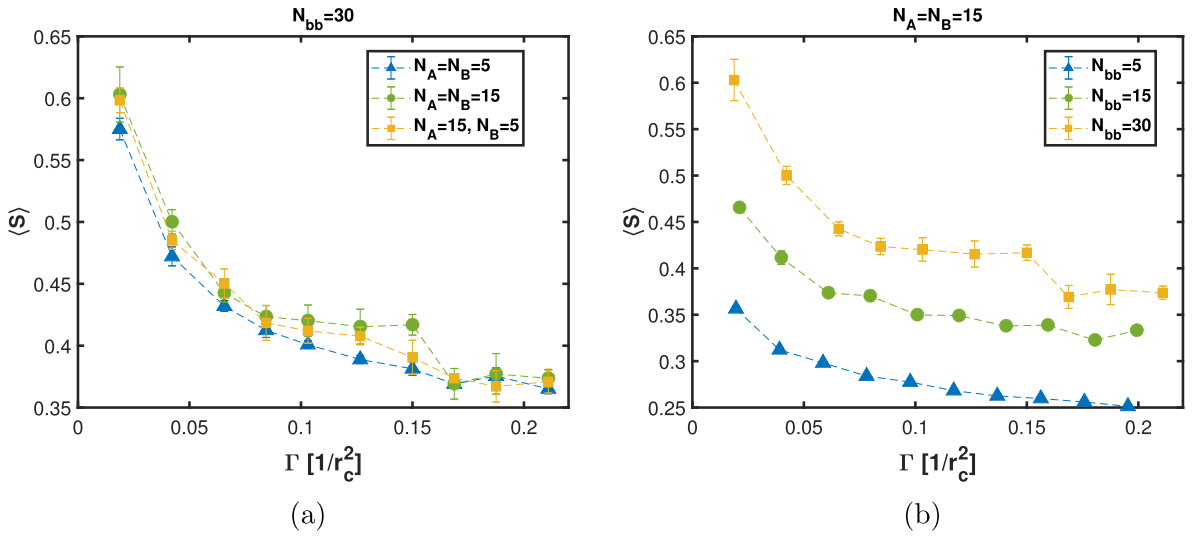

Figure 7. Orientational order parameter as a function of surface concentration. (a) Fixed backbone length (N_{bb} = 30) with varying side chain length. (b) Fixed side chain length (N_A = N_B = 15) with varying backbone length. The global orientational order decreases as the surface concentration increases. Note that long backbone lengths favor larger values of $\langle S \rangle$. For some curves, error bars are smaller than the symbols.

backbones and reducing $\langle R_{bb} \rangle$. A similar behavior for the backbone end-to-end distance for N_{bb} = 15 is shown in Figure S7. To elucidate the conformations adopted by side chains as the interface saturates, the parallel and perpendicular components, with respect to the interface, of the end-to-end vector associated with each side chain were computed. As before, when side chains are short, the effect of surface concentration is not strong, and little variation is observed in both parallel and perpendicular components of the end-to-end vector for both types of side chains (see Figure 6). Note that side chains are mostly lying along the interface with a small perpendicular component. In the case of large side chains, as Γ increases, the parallel component decreases at the same time as the perpendicular component increases, indicating that side chains stretch away from the interface to avoid overlaps, as expected for polymer brushes at high coverage on an interface.[67] At low concentrations, side chains prefer to lie parallel to the interface, and this is favored by the fact that the incompatibility between side chains and opposite solvents is weaker than the oil−water repulsion. Thus, the side chain chemistry can also be used to achieve control of side chain conformations at the liquid−liquid interface.

Orientational Order. The next task was to investigate the collective organization of bottlebrushes at the interface. To do so, the orientational order parameter, S, associated with the backbones, was computed as a function of surface concentration (Figure 7). In accordance with the phenomenology described above, $\langle S \rangle$ decreases, from values close to 0.6 to values close to 0.35, as Γ increases: at low polymer surface concentration, bottlebrushes adopt cylindrical morphologies with extended backbones, due to their higher emergent topological stiffness, which would favor the alignment of bottlebrushes and large values of the order parameter $\langle S \rangle$. As polymers start overlapping and excluded volume interactions reduce, backbones adopt both extended and folded conformations, which produces just local order (segments of polymers aligned in the same direction, see snapshots in Figure 2) but global order reduces, giving place to low values of the order parameter $\langle S \rangle$. Now, in the low dilution limit where polymers do not interact with each other, the order parameter should be zero. Thus, one would expect that the curve $\langle S \rangle$ vs Γ will display a maximum at some Γ* value; such a maximum is not present in our data. Clearly, simulations in the low dilution limit are needed; however, it is suspected that finite-size effects (due to the small number of polymers in the samples) are strong, which might give rise to large $\langle S \rangle$ values at low concentrations. Thus, one should be careful when interpreting the results presented in Figure 7; data in Figure 5a (and Figure S9) suggest that, for a fixed backbone length, side chain degree of polymerization does not affect the orientational order in a significant manner. On the other hand, backbone length has a pronounced effect on the orientational order. As can be seen in Figure 5b, the orientational order parameter increases systematically as the backbone length increases, which agrees with the expected behavior of rigid rods that display lyotropic nematic phases for long-enough rods. However, the analogy should not be taken literally since, as discussed above, bottlebrushes' effective stiffness depends on polymer concentration. To summarize, as polymer surface concentration increases, bottlebrushes lose global orientational correlation, but local orientational order remains, and it is larger for polymers with long backbones.

Surface-Active Properties. We now turn to the thermodynamic interfacial properties. The effect of the polymer architecture and Γ on the interfacial tension, γ_{int}, was elucidated from the calculation of the pressure tensor (as described in the Methods section), and it is shown in Figure 8 for both N_{bb} = 5 and N_{bb} = 30. As expected, the interfacial tension decreases as Γ increases, showing that bottlebrushes can stabilize the O/W interfaces. Furthermore, it can be observed that the brush polymers that have the most reduction are the ones with long symmetric side chains, N_A = N_B = 15, whereas symmetric brushes with short side chains, N_A = N_B = 5, had the least reduction in γ_{int}. Asymmetric bottlebrushes reduce γ_{int} to values between the two symmetric cases. To see the effect of backbone length more clearly, Figure 9 displays the curves γ_{int} vs Γ for all cases in Figure 8. Yellow curves correspond to large backbones (N_{bb} = 30), and blue curves correspond to short backbones (N_{bb} = 5). As can be seen, at a fixed Γ, shorter backbones reduce interfacial tension even further than long backbones (with side chains of the same length). These results are in agreement with experimental observations by Hsieh et al.,[28] where it was found

https://doi.org/10.1021/acs.macromol.3c02278
Macromolecules 2024, 57, 2773−2785

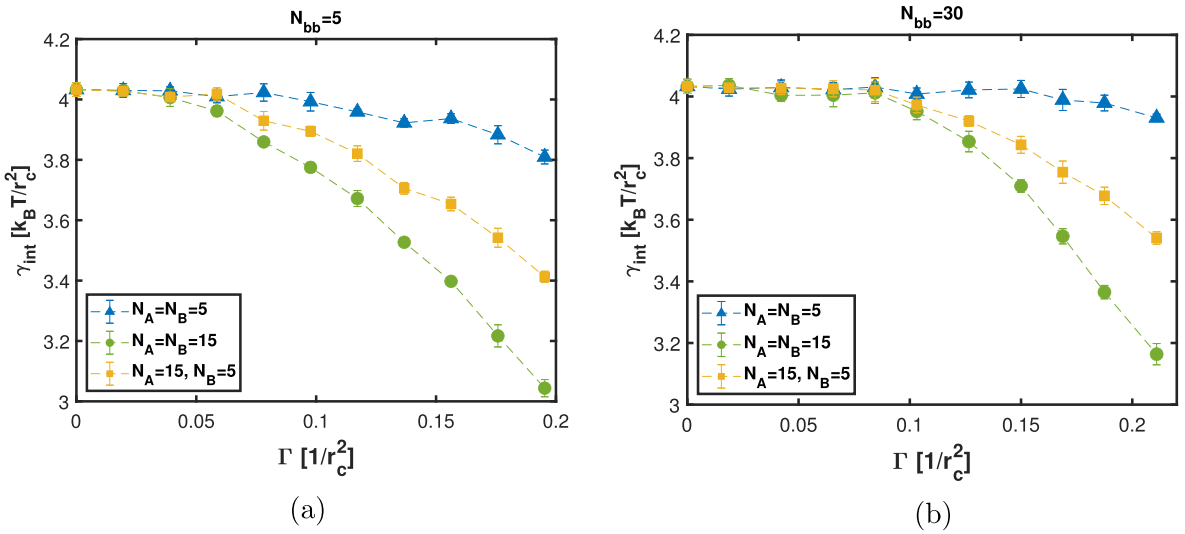

Figure 8. Interfacial tension as a function of surface concentration for two backbone lengths (a) N_{bb} = 5 and (b) N_{bb} = 30. The interfacial tension for both backbone lengths decreases as the interface gets saturated by brush polymers. Note the stronger reduction achieved by long side chains compared to short side chains.

that short backbones and high PEO content give rise to a stronger reduction of γ_{int}, compared to brush polymers with long

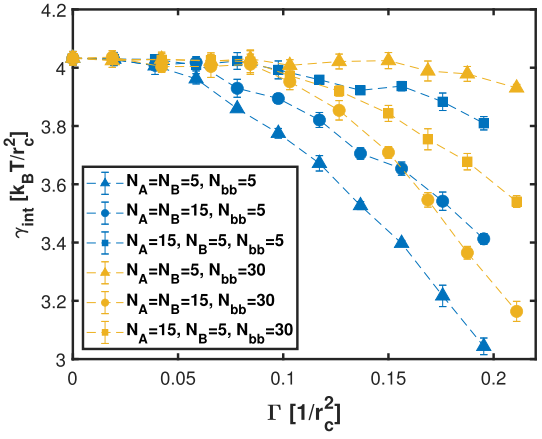

Figure 9. Effect of backbone length on the interfacial tension. Two different lengths are compared, N_{bb} = 5 and N_{bb} = 30. Long side chains and short backbones favor a stronger decrease of γ_{int}, as found experimentally by Hsieh et al.[28]

backbones and low POE content. Simulation results in Figure 9 also agree with the experimental findings of Seong et al.;[29] these authors found that for fully grafted polymers with symmetric composition (f_{POE} = 0.5), the larger N_{bb} is, the less reduction of interfacial tension is achieved. It should be noted here that to ensure that there were no finite-size effects on γ_{int} due to the size of the simulation box, the interfacial tension for N_{bb} = 30 with N_A = N_B = 15 was computed using different box sizes. It was found that very little to no difference in the values of γ_{int} were present, as shown in Figure S12.

From the results described above, one could conclude that short backbones with long side chains are better to achieve more stable liquid−liquid interfaces since a lower surface tension is achieved for the same total mass of polymer. However, Hsieh et al.[28] reported that interfacial rheology seems to play a more important role regarding the stabilization of emulsions. Their experiments suggest that the most efficient bottlebrush emulsifiers are those that produce interfacial stiffening.[28] Taking this into consideration, surface-related mechanical properties were estimated; first, the surface pressure $\Pi \equiv \gamma_0 - \gamma_{int}$ was computed as a function of the molecular area, defined as $A \equiv 1/\Gamma$. The corresponding curves are displayed in Figure 10; as can be seen, a greater surface pressure is induced by longer side chains. It can also be noticed that the rate of change of Π with respect to Γ seems to depend on both side chain and backbone lengths. Thus, we computed the Gibbs dilatational elasticity, E, defined as[28] $E \equiv (\partial\Pi_e/\partial \ln \Gamma)_{N,T}$, where Π_e is the equilibrium surface pressure; numerical differentiation was used to compute E for the different systems in Figure 10. It should be noted that the Gibbs elasticity is not comparable with the dynamic dilatational modulus reported by Hsieh et al.[28] The former is an elastic constant defined for systems at equilibrium, and the latter comes from rheological measurements. As can be seen in Figure 11, long side chains give rise to a larger Gibbs elastic modulus compared to short and asymmetric side chains. The effect of the backbone length is more clear in Figure 12: the data indicates that short bottlebrushes with short and asymmetric side chains give rise to larger Gibbs elasticity compared to long bottlebrushes. However, at high surface concentrations, long bottlebrushes with large side chains give rise to a modulus that is slightly larger than that of short bottlebrushes with long side chains. A more detailed analysis regarding interfacial mechanical properties, both at- and out-of-equilibrium, is required to have a better comprehension of the effect of architectural parameters on these properties and their influence on the stability of emulsions.

We conclude this section by noticing that polymer flexibility has a strong influence on the conformations that polymers can adopt, and therefore, interfacial properties would also be affected by macromolecular flexibility. In this work, a fully flexible model, for both side chains and backbones, was used; an emergent stiffness arises from the interactions between side chains, but our bottlebrushes are intrinsically flexible. Using a fully flexible model reduces the computational cost, but more importantly, our goal was to represent polymers with small persistence lengths; thus, given the coarse-grained approach used here, a flexible model is a good approximation. However,

https://doi.org/10.1021/acs.macromol.3c02278
Macromolecules 2024, 57, 2773−2785

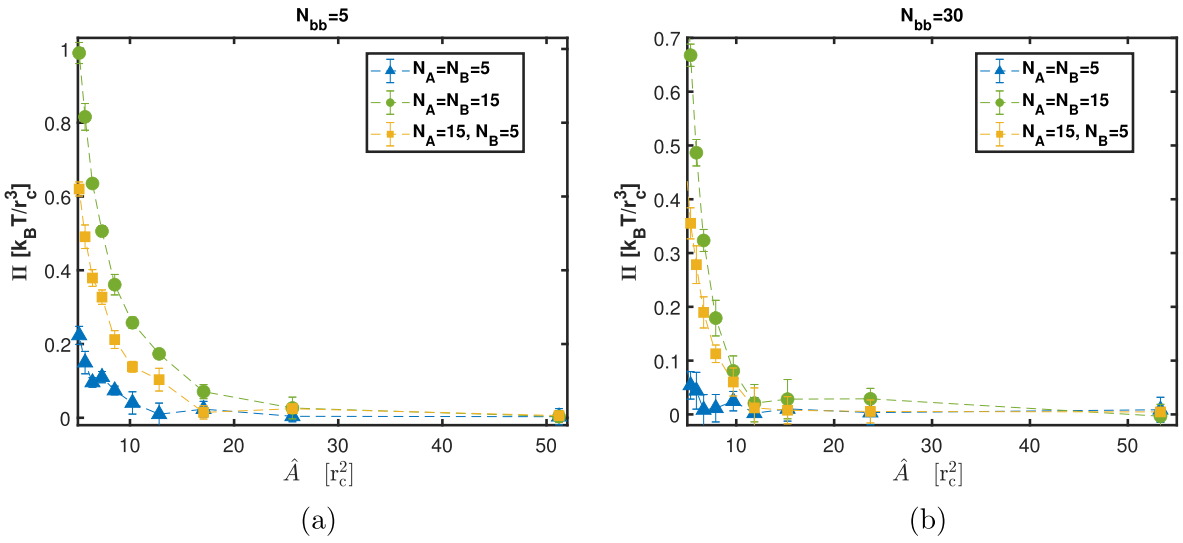

Figure 10. Interfacial pressure as a function of the molecular area $\hat{A}$. Two different backbone lengths are compared (a) N_{bb} = 5 and (b) N_{bb} = 30. The interfacial pressure for both backbone lengths increases as $\hat{A}$ decreases, or equivalently, as the number of brush polymers increases at the interface.

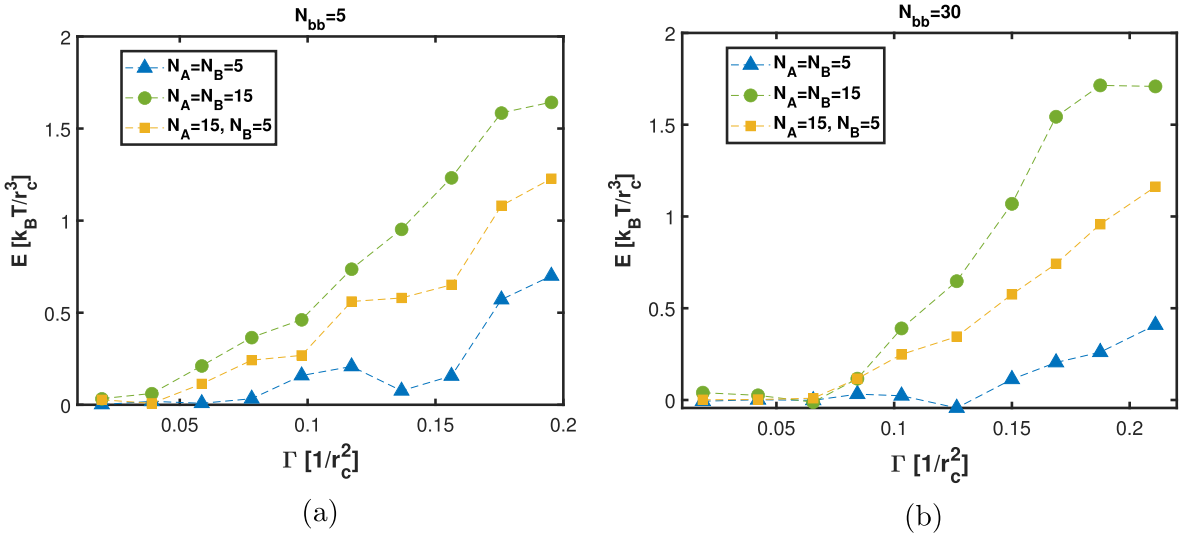

Figure 11. Gibbs elastic modulus, E, as a function of surface concentration for two backbone lengths (a) N_{bb} = 5 and (b) N_{bb} = 30. Long side chains give rise to a larger modulus.

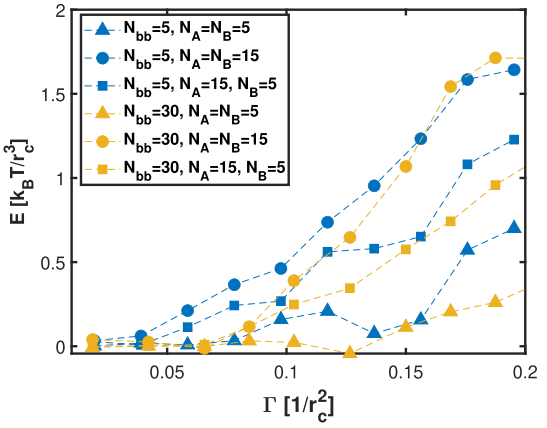

Figure 12. Effect of backbone length on the Gibbs elastic modulus, E. Two different lengths are compared, N_{bb} = 5 and N_{bb} = 30.

polymers with a large persistence length, both at the backbone or side chain level, will adopt more rigid conformations, which could, potentially, allow for a better packing at the liquid−liquid interface, thus reducing interfacial tension more than flexible polymers; polymer rigidity could also affect the surface rheology. Therefore, a systematic study of the effect of polymer flexibility on the results presented in this work is warranted.

CONCLUSIONS

Extensive DPD simulations have been performed to elucidate the effect of side chain and backbone lengths, as well as polymer surface concentration, on the structure and organization of amphiphilic mikto-grafted molecular brushes at liquid−liquid planar interfaces. Our simulation results show that at low surface concentrations, brush polymers adopt elongated conformations with extended backbones, and these conformations are favored when side chains are long. Under low-concentration conditions, side chains adopt conformations lying, mostly, along the interface. As concentration increases, two effects arise: on the

https://doi.org/10.1021/acs.macromol.3c02278
Macromolecules 2024, 57, 2773−2785

one hand, backbones no longer adopt extended conformations only but also display folded conformations, thus reducing backbone end-to-end distances and shape anisotropy. On the other hand, side chains transit to conformations where the parallel component of their end-to-end vector reduces at the same time as their perpendicular component increases, as expected for polymer brushes at high-grafting densities on solid surfaces. At the collective organization level, it was found that the global orientational order is reduced as polymer surface concentration is increased; however, local order remains, and it is higher for brush polymers with large backbones. Finally, thermodynamic interfacial properties were computed, and simulation results predict that bottlebrushes with long side chains and small backbones are better at reducing interfacial tension compared to polymers with long backbones and short side chains; this is in agreement with previous experimental observations. However, experimental data suggest that thermodynamics does not seem to be the only factor involved in the stability of emulsions, and interfacial rheological properties are also quite relevant. We have computed the Gibbs elastic modulus and found that large backbones seem to give rise to larger values of this mechanical quantity at high concentrations compared to polymers with short backbones. This might suggest that bottlebrushes with long backbones and long side chains are better emulsifiers; however, more detailed analysis of mechanical and rheological properties is needed to reach a definite understanding. The results reported here provide structure-interfacial property relations that will be useful to have a deeper understanding of how the molecular engineering of amphiphilic mikto-grafted molecular brushes will affect their behavior at oil−water interfaces to create advanced responsive emulsions.

■ ASSOCIATED CONTENT

Supporting Information

The Supporting Information is available free of charge at https://pubs.acs.org/doi/10.1021/acs.macromol.3c02278.

All concentration values explored in this work; representative snapshots and density profiles for backbones N_{bb} = 30 and 5, for different side chain lengths; morphological properties, and orientational order parameter and interfacial properties for N_{bb} = 15 (PDF)

■ AUTHOR INFORMATION

Corresponding Author

Abelardo Ramírez-Hernández − *Department of Biomedical Engineering and Chemical Engineering, The University of Texas at San Antonio, San Antonio, Texas 78249, United States; Department of Physics and Astronomy, The University of Texas at San Antonio, San Antonio, Texas 78249, United States;* orcid.org/0000-0002-3569-5223; Email: abelardo.ramirez-hernandez@utsa.edu

Authors

Carlos A. Salinas-Soto − *Department of Biomedical Engineering and Chemical Engineering, The University of Texas at San Antonio, San Antonio, Texas 78249, United States; Department of Physics and Astronomy, The University of Texas at San Antonio, San Antonio, Texas 78249, United States*

Carlos Padilla-Gutierrez − *Department of Biomedical Engineering and Chemical Engineering, The University of Texas at San Antonio, San Antonio, Texas 78249, United States*

Margarita Herrera-Alonso − *Chemical & Biological Engineering & School of Advanced Materials Discovery, Colorado State University, Fort Collins, Colorado 80523, United States;* orcid.org/0000-0002-6064-8699

Esteban E. Ureña-Benavides − *Department of Biomedical Engineering and Chemical Engineering, The University of Texas at San Antonio, San Antonio, Texas 78249, United States;* orcid.org/0000-0002-5525-488X

Complete contact information is available at: https://pubs.acs.org/10.1021/acs.macromol.3c02278

Notes

The authors declare no competing financial interest.

■ ACKNOWLEDGMENTS

This research was funded in part by a grant from The Welch Foundation to A.R.-H. (Grant no. AX-2119-20220331). M.H.-A. acknowledges the support of the National Science Foundation through grant NSF 2003789. We gratefully acknowledge the computing resources provided at ARC, a high-performance computing cluster operated by the Office of Information Technology at UTSA. The authors are also grateful for valuable computing resources provided by the Texas Advanced Computing Center (TACC) at The University of Texas at Austin (URL: http://www.tacc.utexas.edu).

■ REFERENCES

(1) Unsal, H.; Onbulak, S.; Calik, F.; Er-Rafik, M.; Schmutz, M.; Sanyal, A.; Rzayev, J. Interplay between molecular packing, drug loading, and core cross-linking in bottlebrush copolymer micelles. *Macromolecules* **2017**, *50*, 1342−1352.

(2) Williford, J.-M.; Santos, J. L.; Shyam, R.; Mao, H.-Q. Shape control in engineering of polymeric nanoparticles for therapeutic delivery. *Biomater. Sci.* **2015**, *3*, 894−907.

(3) Verduzco, R.; Li, X.; Pesek, S. L.; Stein, G. E. Structure, function, self-assembly, and applications of bottlebrush copolymers. *Chem. Soc. Rev.* **2015**, *44*, 2405−2420.

(4) Bodratti, A. M.; Alexandridis, P. Amphiphilic block copolymers in drug delivery: Advances in formulation structure and performance. *Expert Opin. Drug Delivery* **2018**, *15*, 1085−1104.

(5) Liberman-Martin, A. L.; Chu, C. K.; Grubbs, R. H. Application of bottlebrush block copolymers as photonic crystals. *Macromol. Rapid Commun.* **2017**, *38*, 1700058.

(6) Lequieu, J.; Quah, T.; Delaney, K. T.; Fredrickson, G. H. Complete Photonic Band Gaps with Nonfrustrated ABC Bottlebrush Block Polymers. *ACS Macro Lett.* **2020**, *9*, 1074−1080.

(7) Benichou, A.; Aserin, A.; Garti, N. Protein-polysaccharide interactions for stabilization of food emulsions. *J. Dispersion Sci. Technol.* **2002**, *23*, 93−123.

(8) Fujisawa, S.; Togawa, E.; Kuroda, K. Nanocellulose-stabilized Pickering emulsions and their applications. *Sci. Technol. Adv. Mater.* **2017**, *18*, 959−971.

(9) Seino, H.; Kawaguchi, N.; Arai, Y.; Ozawa, N.; Hamada, K.; Nagao, N. Investigation of partially myristoylated carboxymethyl chitosan, an amphoteric-amphiphilic chitosan derivative, as a new material for cosmetic and dermal application. *J. Cosmet. Dermatol.* **2021**, *20*, 2332−2340.

(10) Viola, M.; Migliorini, C.; Matricardi, P.; Di Meo, C. Synthesis and characterization of a novel amphiphilic polyacrylate-cholesterol derivative as promising material for pharmaceutical and cosmetic applications. *Eur. Polym. J.* **2023**, *184*, 111774.

(11) Tian, S.; Gao, W.; Liu, Y.; Kang, W. Study on the stability of heavy crude oil-in-water emulsions stabilized by two different

hydrophobic amphiphilic polymers. *Colloids Surf., A* **2019**, *572*, 299−306.
(12) Sun, J.; Xu, X.; Wang, J.; Zhang, W.; Yang, H.; Jing, X.; Shi, X. Synthesis and emulsification properties of an amphiphilic polymer for enhanced oil recovery. *J. Dispersion Sci. Technol.* **2010**, *31*, 931−935.
(13) Raffa, P.; Broekhuis, A. A.; Picchioni, F. Polymeric surfactants for enhanced oil recovery: A review. *J. Pet. Sci. Eng.* **2016**, *145*, 723−733.
(14) Torcello-Gómez, A.; Wulff-Pérez, M.; Gálvez-Ruiz, M. J.; Martín-Rodríguez, A.; Cabrerizo-Vílchez, M.; Maldonado-Valderrama, J. Block copolymers at interfaces: Interactions with physiological media. *Adv. Colloid Interface Sci.* **2014**, *206*, 414−427.
(15) Wyman, I.; Njikang, G.; Liu, G. When emulsification meets self-assembly: The role of emulsification in directing block copolymer assembly. *Prog. Polym. Sci.* **2011**, *36*, 1152−1183.
(16) Kuperkar, K.; Patel, D.; Atanase, L. I.; Bahadur, P. Amphiphilic block copolymers: their structures, and self-assembly to polymeric micelles and polymersomes as drug delivery vehicles. *Polymers* **2022**, *14*, 4702.
(17) Li, Z.; Ma, J.; Cheng, C.; Zhang, K.; Wooley, K. L. Synthesis of Hetero-Grafted Amphiphilic Diblock Molecular Brushes and Their Self-Assembly in Aqueous Medium. *Macromolecules* **2010**, *43*, 1182−1184.
(18) Zhao, L.; Lin, Z. Self-assembly of non-linear polymers at the air/water interface: the effect of molecular architecture. *Soft Matter* **2011**, *7*, 10520−10535.
(19) Li, W.; Yu, Y.; Lamson, M.; Silverstein, M. S.; Tilton, R. D.; Matyjaszewski, K. PEO-Based Star Copolymers as Stabilizers for Water-in-Oil or Oil-in-Water Emulsions. *Macromolecules* **2012**, *45*, 9419−9426.
(20) Li, Y.; Zou, J.; Das, B. P.; Tsianou, M.; Cheng, C. Well-Defined Amphiphilic Double-Brush Copolymers and Their Performance as Emulsion Surfactants. *Macromolecules* **2012**, *45*, 4623−4629.
(21) Xie, G.; Krys, P.; Tilton, R. D.; Matyjaszewski, K. Heterografted molecular brushes as stabilizers for water-in-oil emulsions. *Macromolecules* **2017**, *50*, 2942−2950.
(22) Chen, K.; Hu, X.; Zhu, N.; Guo, K. Design, Synthesis, and Self-Assembly of Janus Bottlebrush Polymers. *Macromol. Rapid Commun.* **2020**, *41*, 2000357.
(23) Hu, M.; Russell, T. P. Polymers with advanced architectures as emulsifiers for multi-functional emulsions. *Mater. Chem. Front.* **2021**, *5*, 1205−1220.
(24) Wang, B.; Liu, T.; Chen, H.; Yin, B.; Zhang, Z.; Russell, T. P.; Shi, S. Molecular brush surfactants: versatile emulsifiers for stabilizing and structuring liquids. *Angew. Chem., Int. Ed.* **2021**, *60*, 19626−19630.
(25) Laws, T. S.; Mei, H.; Terlier, T.; Verduzco, R.; Stein, G. E. Tailoring the Wettability and Substrate Adherence of Thin Polymer Films with Surface-Segregating Bottlebrush Copolymer Additives. *Langmuir* **2023**, *39*, 7201−7211.
(26) Huang, Y.-R.; Lamson, M.; Matyjaszewski, K.; Tilton, R. D. Enhanced interfacial activity of multi-arm poly(ethylene oxide) star polymers relative to linear poly(ethylene oxide) at fluid interfaces. *Phys. Chem. Chem. Phys.* **2017**, *19*, 23854−23868.
(27) Olszewski, M.; Hu, X.; Lin, T.-C.; Matyjaszewski, K.; Lebedeva, N.; Taylor, P. Oscillatory and Relaxation Study of the Interfacial Rheology of Star Polymers with Low-Grafting-Density PEO Arms and Hydrophobic Poly(divinylbenzene) Cores. *Langmuir* **2023**, *39*, 7741−7758.
(28) Hsieh, T.-L.; Martinez, M. R.; Garoff, S.; Matyjaszewski, K.; Tilton, R. D. Interfacial dilatational rheology as a bridge to connect amphiphilic heterografted bottlebrush copolymer architecture to emulsifying efficiency. *J. Colloid Interface Sci.* **2021**, *581*, 135−147.
(29) Seong, H.-G.; Chen, Z.; Emrick, T.; Russell, T. P. Reconfiguration and reorganization of bottlebrush polymer surfactants. *Angew. Chem.* **2022**, *134*, No. e202200530.
(30) Shandiz, S. A.; Leuty, G. M.; Guo, H.; Mokarizadeh, A. H.; Maia, J. M.; Tsige, M. Structure and Thermodynamics of Linear, Ring, and Catenane Polymers in Solutions and at Liquid−Liquid Interfaces. *Langmuir* **2023**, *39*, 7154−7166.
(31) Borówko, M.; Staszewski, T.; Tomasik, J. Janus Ligand-Tethered Nanoparticles at Liquid−Liquid Interfaces. *J. Phys. Chem. B* **2023**, *127*, 5150−5161.
(32) Bugaeva, A. S.; Gumerov, R. A.; Potemkin, I. I. Morphological Transitions in Micelles of Amphiphilic Bottlebrushes upon the Adsorption and Compression at the Liquid Interface. *Polymers* **2022**, *14*, 5076.
(33) Moghimikheirabadi, A.; Ilg, P.; Sagis, L. M.; Kroger, M. Surface rheology and structure of model triblock copolymers at a liquid−vapor interface: A molecular dynamics study. *Macromolecules* **2020**, *53*, 1245−1257.
(34) Moghimikheirabadi, A.; Fischer, P.; Kröger, M.; Sagis, L. M. C. Relaxation Behavior and Nonlinear Surface Rheology of PEO−PPO−PEO Triblock Copolymers at the Air−Water Interface. *Langmuir* **2019**, *35*, 14388−14396.
(35) Gartner, T. E., III; Jayaraman, A. Modeling and simulations of polymers: a roadmap. *Macromolecules* **2019**, *52*, 755−786.
(36) Mohammadi, E.; Joshi, S. Y.; Deshmukh, S. A. A review of computational studies of bottlebrush polymers. *Comput. Mater. Sci.* **2021**, *199*, 110720.
(37) Zhu, Q.; Tree, D. R. Simulations of morphology control of self-assembled amphiphilic surfactants. *J. Polym. Sci.* **2023**, *61*, 1214−1240.
(38) Hoogerbrugge, P.; Koelman, J. Simulating microscopic hydrodynamic phenomena with dissipative particle dynamics. *Europhys. Lett.* **1992**, *19*, 155−160.
(39) Español, P.; Warren, P. B. Perspective: Dissipative particle dynamics. *J. Chem. Phys.* **2017**, *146*, 150901.
(40) Groot, R. D.; Warren, P. B. Dissipative particle dynamics: Bridging the gap between atomistic and mesoscopic simulation. *J. Chem. Phys.* **1997**, *107*, 4423−4435.
(41) Wright, D. B.; Ramírez-Hernández, A.; Touve, M. A.; Carlini, A. S.; Thompson, M. P.; Patterson, J. P.; de Pablo, J. J.; Gianneschi, N. C. Enzyme-Induced Kinetic Control of Peptide−Polymer Micelle Morphology. *ACS Macro Lett.* **2019**, *8*, 676−681.
(42) Zhu, Q.; Scott, T. R.; Tree, D. R. Using reactive dissipative particle dynamics to understand local shape manipulation of polymer vesicles. *Soft Matter* **2021**, *17*, 24−39.
(43) Harmat, A. L.; Javan Nikkhah, S.; Sammalkorpi, M. Dissipative particle dynamics simulations of H-shaped diblock copolymer self-assembly in solvent. *Polymer* **2021**, *233*, 124198.
(44) Santo, K. P.; Neimark, A. V. Dissipative particle dynamics simulations in colloid and Interface science: A review. *Adv. Colloid Interface Sci.* **2021**, *298*, 102545.
(45) Wang, J.; Han, Y.; Xu, Z.; Yang, X.; Ramakrishna, S.; Liu, Y. Dissipative particle dynamics simulation: A review on investigating mesoscale properties of polymer systems. *Macromol. Mater. Eng.* **2021**, *306*, 2000724.
(46) Guo, W. X.; Hu, L. F.; Feng, Y. H.; Chen, B. Z.; Guo, X. D. Advances in self-assembling of pH-sensitive polymers: A mini review on dissipative particle dynamics. *Colloids Surf., B* **2022**, *210*, 112202.
(47) Procházka, K.; Limpouchová, Z.; Štěpánek, M.; Šindelka, K.; Lísal, M. DPD Modelling of the Self-and Co-Assembly of Polymers and Polyelectrolytes in Aqueous Media: Impact on Polymer Science. *Polymers* **2022**, *14*, 404.
(48) Javan Nikkhah, S.; Sammalkorpi, M. Single core and multicore aggregates from a polymer mixture: A dissipative particle dynamics study. *J. Colloid Interface Sci.* **2023**, *635*, 231−241.
(49) Kim, T.-Y.; Hur, S.-M.; Ramírez-Hernández, A. Effect of Block Sequence on the Solution Self-Assembly of Symmetric ABCBA Pentablock Polymers in a Selective Solvent. *J. Phys. Chem. B* **2023**, *127*, 2575−2586.
(50) Gumus, B.; Herrera-Alonso, M.; Ramírez-Hernández, A. Kinetically-arrested single-polymer nanostructures from amphiphilic mikto-grafted bottlebrushes in solution: A simulation study. *Soft Matter* **2020**, *16*, 4969−4979.
(51) Salinas-Soto, C. A.; Leon-Islas, J. G.; Herrera-Alonso, M.; Ramírez-Hernández, A. Hydrophobic Solute Encapsulation by Amphiphilic Mikto-Grafted Bottlebrushes: A Dissipative Particle Dynamics Study. *ACS Appl. Polym. Mater.* **2022**, *4*, 7340−7351.

https://doi.org/10.1021/acs.macromol.3c02278
Macromolecules 2024, 57, 2773−2785

(52) Ahmadi, M.; Aliabadian, E.; Liu, B.; Lei, X.; Khalilpoorkordi, P.; Hou, Q.; Wang, Y.; Chen, Z. Comprehensive review of the interfacial behavior of water/oil/surfactant systems using dissipative particle dynamics simulation. *Adv. Colloid Interface Sci.* **2022**, *309*, 102774.
(53) Phillips, C. L.; Anderson, J. A.; Glotzer, S. C. Pseudo-random number generation for Brownian Dynamics and Dissipative Particle Dynamics simulations on GPU devices. *J. Comput. Phys.* **2011**, *230*, 7191−7201.
(54) Glaser, J.; Nguyen, T. D.; Anderson, J. A.; Lui, P.; Spiga, F.; Millan, J. A.; Morse, D. C.; Glotzer, S. C. Strong scaling of general-purpose molecular dynamics simulations on GPUs. *Comput. Phys. Commun.* **2015**, *192*, 97−107.
(55) Humphrey, W.; Dalke, A.; Schulten, K. VMD: visual molecular dynamics. *J. Mol. Graphics* **1996**, *14*, 33−38.
(56) Gowers, R. J.; Linke, M.; Barnoud, J.; Reddy, T. J.; Melo, M. N.; Seyler, S. L.; Domanski, J.; Dotson, D. L.; Buchoux, S.; Kenney, I. M.; et al. MDAnalysis: a Python package for the rapid analysis of molecular dynamics simulations. In *Proceedings of the 15th python in science conference*, 2016; p 105.
(57) Michaud-Agrawal, N.; Denning, E. J.; Woolf, T. B.; Beckstein, O. MDAnalysis: a toolkit for the analysis of molecular dynamics simulations. *J. Comput. Chem.* **2011**, *32*, 2319−2327.
(58) Arkın, H.; Janke, W. Gyration tensor based analysis of the shapes of polymer chains in an attractive spherical cage. *J. Chem. Phys.* **2013**, *138*, 054904.
(59) Blavatska, V.; Janke, W. Shape anisotropy of polymers in disordered environment. *J. Chem. Phys.* **2010**, *133*, 184903.
(60) Theodorou, D. N.; Suter, U. W. Shape of unperturbed linear polymers: polypropylene. *Macromolecules* **1985**, *18*, 1206−1214.
(61) Rowlinson, J.; Widom, B. *Molecular Theory of Capillarity*. *Dover books on chemistry*; Dover Publications, 2002.
(62) Andrienko, D. Introduction to liquid crystals. *J. Mol. Liq.* **2018**, *267*, 520−541.
(63) Salinas-Soto, C. A.; Choe, Y.; Hur, S.-M.; Ramírez-Hernández, A. Exploring conformations of comb-like polymers with varying grafting density in dilute solutions. *J. Chem. Phys.* **2023**, *159*, 114901.
(64) Morozova, S.; Lodge, T. P. Conformation of Methylcellulose as a Function of Poly(ethylene glycol) Graft Density. *ACS Macro Lett.* **2017**, *6*, 1274−1279.
(65) Tang, Z.; Pan, X.; Zhou, H.; Li, L.; Ding, M. Conformation of a Comb-like Chain Free in Solution and Confined in a Nanochannel: From Linear to Bottlebrush Structure. *Macromolecules* **2022**, *55*, 8668−8675.
(66) Paturej, J.; Kreer, T. Hierarchical excluded volume screening in solutions of bottlebrush polymers. *Soft Matter* **2017**, *13*, 8534−8541.
(67) Milner, S. T. Polymer Brushes. *Science* **1991**, *251*, 905−914.
(68) Frenkel, D.; Smit, B. *Understanding Molecular Simulation: From Algorithms to Applications*; Elsevier, 2002.

https://doi.org/10.1021/acs.macromol.3c02278
Macromolecules 2024, 57, 2773−2785